Density Functional Study and Normal-Mode Analysis of the Bindings and Vibrational Frequency Shifts of the Pyridine−M (M = Cu, Ag, Au, Cu^+, Ag^+, Au^+, and Pt) Complexes

De-Yin Wu,*,† Bin Ren,† Yu-Xiong Jiang,† Xin Xu,‡ and Zhong-Qun Tian*,‡

Department of Chemistry, Xiamen University, Xiamen 361005, China, and State Key Laboratory for Physical Chemistry of Solid Surfaces, Xiamen University, Xiamen 361005, China

Received: April 19, 2002; In Final Form: July 15, 2002

Raman and infrared (IR) spectroscopies have been used extensively to study the adsorption of pyridine on various surfaces for more than 40 years. However, no satisfactory assignment on all the vibrational modes has been achieved. In the present study, density functional theory at the level of B3LYP/6-311+G** (for C, N, H)/LANL2DZ (for metals) has been used for the normal coordinate calculations of the neutral and cationic species of the pyridine−metal atom (ion) complexes. Based on the present calculations, new assignments of the fundamental frequencies for the bands attributed to υ_{17a}, υ_3, υ_5, and υ_{18b} modes of the free pyridine in the reported IR and Raman spectra have been suggested. The calculated frequency shifts indicate that the coupling among υ_1, υ_{12}, and υ_{18a} modes and the coupling between these modes and the N−metal (Cu, Ag, Au, or Pt) bond depend on the strength of the N−metal bond and its bonding properties. The fundamental frequency of the υ_{6a} mode has a nearly linear relationship with the change of the force constant of the N−M bond. Therefore, its frequency shift can be used to directly correlate to the strength of the interaction of pyridine with the metal atom (surface).

Introduction

Quantum chemical calculation has become an important complement to experiments for assigning the normal modes in the vibrational spectra and the electronic excitation spectra associated with the observed spectroscopic bands. To obtain the vibrational spectra of adsorbates, one may use infrared spectroscopy (IR), Raman spectroscopy, electron energy-loss spectroscopy (EELS), sum-frequency generation (SFG), and difference-frequency generation (DFG).[1−3] To obtain the electronic spectra of adsorbates, one may use UV−vis absorption and fluorescence spectroscopy, two-photon photoemission, EELS, and resonance Raman spectroscopy.[1−4] Pyridine, which may be regarded as a good probe molecule since it is a strong electron donor due to the existence of a lone pair of electrons on the nitrogen atom, has been reported in a number of studies.[5−12] The vibrational frequency shifts of the internal modes, which are sensitive to the interaction between pyridine and an electron acceptor, reflect the nature of the interaction of donor−acceptor and are indicative of the change of the acceptor properties.[11,13−15] In the Raman spectroscopy, the electron excitation results in resonance enhancement of the Raman signal. If an object molecule adsorbs on a metal surface, the enhancement effect of the metal surface as well as the resonance Raman effect of the molecule can be used for the detection of a single molecule and a small amount of medical molecules.[16,17]

The vibrational frequency shifts of the pyridine internal modes in the hydrogen-bonded complexes by the N-end interaction have been reported by many groups.[18−27] These studies show that the strong hydrogen bond results in a blueshift of the ring breath mode of the pyridine molecule. For example, in the pyridine−water complexes, this mode blueshifts to the limit value of 1002 cm^{-1} with the increase in the ratio of pyridine to the water molecules.[18−21] In the pyridine−methanol hydrogen-bonded complexes, a similar phenomenon has been found, indicating that the extent of the blueshift depends on the strength of the hydrogen bond.[22−24]

The vibrational frequency shifts of the pyridine molecule adsorbed on metal and metal oxide surfaces have been investigated even more extensively.[11,14,15,28,29] More than 700 papers on the Raman and IR study of pyridine adsorbed at surfaces have been published in the past over 40 years. For pyridine adsorbed on the gas/solid metal surfaces, the vibrational frequency of the ring breath mode blueshifts to about 1003 and 1010 cm^{-1} on the smooth[30,31] and the rough[32,33] silver surfaces, respectively. For pyridine adsorbed at the liquid/solid metal interfaces, especially at the electrochemical interfaces, the vibrational frequency shifts are very sensitive to the changes of the electrode potentials and the properties of the electrode material.[34−36] For example, there exist large differences either in the relative band intensity or the band frequency between the investigated systems. In our group, especially in recently years, we investigated systematically the surface Raman spectra of pyridine on various coinage metal (including Ag, Au, and Cu) and transition-metal (Fe, Co, Ni, Ru, Rh, and Pt) surfaces.[37−41] The experimental results revealed that the spectral features of pyridine on metal surfaces are really complicated. So far, no satisfactory assignments on the vibrational modes have been achieved. A quantitative explanation to the great spectral differences on the different metal surfaces is still lacking. By only considering electromagnetic (EM) enhancement and charge transfer (CT) enhancement mechanisms for SERS,[7,8] people have not been able to interpret the spectral features of pyridine from different metals. Thus, it is worthwhile to reinvestigate this model system from a more fundamental point

* Authors to whom correspondance should be sent: Z.-Q.T.: telephone, +86-592-2181906; fax, +86-592-2183047; e-mail, zqtian@xmu.edu.cn. D.-Y.W.: e-mail, dywu@jingxian.xmu.edu.cn.

† Department of Chemistry.

‡ State Key Laboratory for Physical Chemistry of Solid Surfaces.

10.1021/jp025970i CCC: $22.00
Published on Web 09/06/2002

of view, i.e., through quantum chemical calculations to assign the normal modes in the vibrational spectra associated with the observed spectroscopic bands.

The main purpose of the present paper is to understand how the vibrational frequency shifts due to the interaction of pyridine with a metal atom through its N-end. At the same time, we will discuss in detail the coupling of the different vibrational modes in the pyridine−metal complexes. The results show that only within the range of the coupling can the strength of the N−M bond significantly influence the frequency of the ring breath vibration. Thus, the present paper is organized in the following manner. The details of the computational methods will be described first. Then, a comparison of the geometric changes in the different pyridine−metal complexes, an analysis of bonding interaction, the calculated frequencies, and their assignments in terms of the potential energy distribution (PED) will be made. Finally, the coupling of the different vibrational modes with the total-symmetric motions and their implications on the bonding mechanism will be discussed.

Computational Details

Geometrical optimizations and vibrational frequency analyses for all neutral and cationic pyridine complexes reported here are performed using B3LYP with *Gaussian 98*.[42,43] For the systems containing the metal atoms or cations, the density function theory (DFT) method, such as B3LYP, is more readily applicable. The basis set for a C, N, or H atom is 6-311+G**, which adds the polarization function to every atom and only adds the diffuse function to a C or N atom. Metal atoms, i.e., Cu, Ag, Au, and Pt, are described by the relativistic LANL2DZ pesudopotentials with a small core approximation, combined with the associated basis functions for the valence electrons.[44]

In the calculations, the spin states for the complexes are assumed to be the same as the ground states for the metal atoms or ions. Thus the Cu, Ag, and Au complexes are doublet with the electronic configuration for the metals as being $(n-1)d^{10}ns^1$, while the Cu^+, Ag^+, and Au^+ complexes are singlet with the electronic configuration of metal ions being $(n-1)d^{10}ns^0$. We find the ground state of the pyridine−Pt complex is a singlet, even though the ground state of the Pt atom is a triplet.[45,46] Thus, a singlet pyridine−Pt complex is adopted in the present calculations. Similar result also appeared in the PtCO complex, which has a singlet ground state, $^1\Sigma^+$.[46] Natural bonding orbital analysis[47] is applied to check the interaction of the lone pair of electrons on the nitrogen atom of pyridine with the metal atoms. All binding energies are corrected by adding a scaled zero-point vibrational energy (ZPVE). Scaled factors for the B3LYP/6-311+G**(C, N, H)/LANL2DZ(M) ZPVE of the pyridine monomer and its complexes are obtained as described in detail in the following.

The local symmetric internal coordinates for the pyridine−metal complexes in the normal-mode analysis are defined using the method given by Pulay et al.[48] and can be found in elsewhere.[49−51] The atom numbering is shown in Figure 1. The DFT force fields are transformed from the Cartesian into the local internal coordinates and then scaled empirically according to the scaled quantum mechanical (SQM) procedure,[52]

$$F_{ij}^{\text{scaled}} = (S_i S_j)^{1/2} F_{ij}^{\text{DFT}}$$

where S_i is the scaled factor of coordinate i, F_{ij}^{DFT} is the B3LYP force constant in the local internal coordinates, and F_{ij}^{scaled} is the scaled force constant. In this study, these scaled factors are initially taken from literature[19] and then fitted by the least-squares procedure to the experimental frequencies in Ar matrix-isolated IR and Raman spectra of free pyridine.[53] The resulting scaled factors are 0.935 for the C−H stretching motions and 0.963 for the ring stretching, bending, and out-of-plane modes, which are used to scale the B3LYP force fields of all the target molecules. For the internal coordinates of the stretching and the bending modes involving the metal atoms, the scaled factors of these force constants are set to be 1.00. The final vibrational frequencies and the potential energy distributions (PEDs) are derived by Wilson's GF matrix method from the SQM DFT force fields.[54]

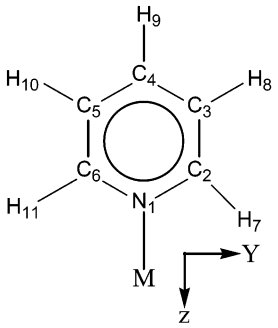

Figure 1. Structure and atomic numbering of pyridine and its metal complexes.

The coupling of the vibrational modes of the total symmetry is analyzed by perturbation of the force constants in a given internal coordinates.[55] To make clear the dependence of the coupling of vibrational modes on the different bonding systems, we select (I) the pyridine−Ag complex, (II) the pyridine−Pt complex, and (III) the pyridine−Cu^+ system and analyze the coupling effect on these three systems. The Py−Ag complex represents a system with a weak σ-donation/π-back-donation interaction; however, the Py−Pt complex belongs to a system having a strong σ-donation/π-back-donation interaction. The third system is different from systems (I) and (II) in that it has not only a strong σ-donation interaction but also a strong electrostatic interaction. The latter effect significantly polarizes the shape of the π electron density of the pyridine ring and thus has an important influence on the spectral properties of the Py−M^+ complexes.

Results and Discussion

Molecular Geometry. The pyridine molecule has a planar structure and belongs to the C_{2V} point group. The structural parameters in the free pyridine have been determined by electron diffraction[56] and microwave spectroscopy.[57] One would normally expect the microwave substitution geometry to be closest to the equilibrium structure of the target molecule. The calculated and experimental structures are listed in Table 1. The CN bond lengths from the microwave experiment are 1.338 Å, the opposite CC bond lengths are 1.392 Å, and the bond lengths of the two paralleled CC bonds are 1.394 Å.[57] Our calculated values are 1.337, 1.392, and 1.394 Å, respectively, which have an error within 0.001 Å as compared to the experimental values. For the CH bonds, the differences between the experimental and theoretical bond lengths are smaller than 0.002 Å. The CNC angle is 116.9° in the microwave structure, and our calculated value is 117.3°. The difference is as small as 0.4°. The good agreement (within 0.2°) between the experiment and the calculation for NCC and two CCC angles of pyridine suggests that the present theoretical level is reliable in reproducing the molecular structures of pyridine. Our B3LYP/6-311+G** geometry for pyridine is clearly superior to that from B3LYP/

TABLE 1: Optimized Bond Distances (in Angstroms) and Bond Angles (in Degrees) of the Ground States of Pyridine and Its Metal Complexes at the B3LYP/6-311+G (for C, N, H)/LANL2DZ (for Metal Atoms) Level**

	expt[a]	Py	Cu	Ag	Au	Cu^+	Ag^+	Au^+	Pt
NM			2.096	2.569	2.391	1.932	2.198	2.056	1.936
NC_2	1.338	1.337	1.342	1.338	1.338	1.352	1.349	1.351	1.357
C_2C_3	1.394	1.394	1.390	1.392	1.391	1.386	1.387	1.385	1.386
C_3C_4	1.392	1.392	1.392	1.392	1.393	1.393	1.392	1.392	1.392
C_2H_7	1.087	1.087	1.085	1.086	1.084	1.082	1.083	1.081	1.079
C_3H_8	1.083	1.084	1.083	1.083	1.083	1.082	1.082	1.082	1.083
C_4H_9	1.082	1.084	1.084	1.084	1.084	1.083	1.083	1.083	1.083
C_6NC_2	116.9	117.3	118.3	118.1	119.1	118.9	119.0	120.3	118.4
NC_2C_3	123.8	123.6	122.7	123.0	122.3	122.0	122.0	121.0	122.0
$C_2C_3C_4$	118.5	118.5	118.8	118.6	118.7	119.1	119.0	119.3	119.7
$C_3C_4C_5$	118.4	118.5	118.7	118.7	118.8	119.0	118.9	119.1	118.1

[a] The experimental data are extracted from Innes et al.[57]

cc-pVDZ, and compares very well to that of B3LYP/cc-pVTZ, where f orbitals were included in the C and N atoms.[58]

For the Py−M^δ complexes, the lengths of the CN bonds and those of the two parallel CC bonds of the pyridine moiety strongly depend on the metal atoms or ions. In the neutral Py−Ag and Py−Au complexes, the CN bonds only lengthen slightly by 0.001 to 1.338 Å. The CN bond length increases significantly to 1.342 Å in the Py−Cu complex. The CN bond lengths in Py−M^+ (M=Cu, Ag, Au) are much longer, ranging from 1.349 to 1.352 Å. The CN bond is the longest (1.357 Å) in Py−Pt. The two parallel CC bonds are apparently shorter in Py−M^δ than those in the pure pyridine. Their bond lengths are within 1.390−1.392 Å for the complexes of Cu, Ag, and Au, and within 1.385−1.387 Å for the Pt complexes and the ion complexes. The other two C−C bond lengths (C_3-C_4/C_4-C_5) are almost unchanged in these complexes. The CNC angle is increased from 117.3° in the free pyridine to 120.3° in the Py−Au^+ complex. Conversely, the NCC angles decrease from 123.6° in the free pyridine to 121.0° in the Py−Au^+ complex. The $C_3C_4C_5$ angles undergo a small change upon forming the complexes. From these geometrical changes, we can conclude that the interactions between pyridine N-end and the metal atoms significantly perturb the bonding in the pyridine molecule around the nitrogen atom.

Experimental Results. Simple and symmetric may the molecular structure of the pyridine molecule seem to be, but the experimental results revealed that the adsorption behavior of pyridine on metal surfaces is really complicated. For example, some selected surface Raman spectra of the adsorbed pyridine at the different surfaces at open circuit potential are given in Figure 2. The potential-dependences of the vibrational frequency of the ν_1 mode of the adsorbed pyridine are presented in Figure 3. As can be seen in the figures, the band frequency for the ν_1 mode at 1007 cm^{-1} on the rough Ag surface is considerably lower than those on the Au and Cu surfaces, locating at 1012 and 1017 cm^{-1} respectively. Although Pt is a transition metal, it presents a quite similar frequency−potential profile as compared to those on the Cu and Au surfaces. Besides the difference in frequency, the difference in the relative intensity of different bands is also quite obvious, as shown in Figure 2. The most striking feature is the great difference in the intensity of the band at about 1035 cm^{-1}, which is the second strongest band for pyridine in the liquid phase. This band is also very strong at the Ag surface, whose intensity is almost equal to that of the ν_1 mode. However, it only exhibits a very weak intensity at around 1038 cm^{-1} at Au and Cu and is almost vanished at the Pt surface. The relative intensity of the 1596 cm^{-1} band of the ν_{8a} mode to the band of the ν_1 mode also depends on the metal entity substantially. We find no satisfactory explanations in the literatures to understand these metal entity-dependent spectral features.[7,8] Moreover, there are some controversies in assigning the vibrational modes of free pyridine. It is therefore necessary to investigate further the surface bonding behavior and recheck the assignment of vibrational properties of pyridine. At this stage, with the abundant experimental data on hand,[53,56−58] it is worthwhile for us to perform more accurate theoretical calculations on the assignment of the vibrational modes of the pyridine molecule.

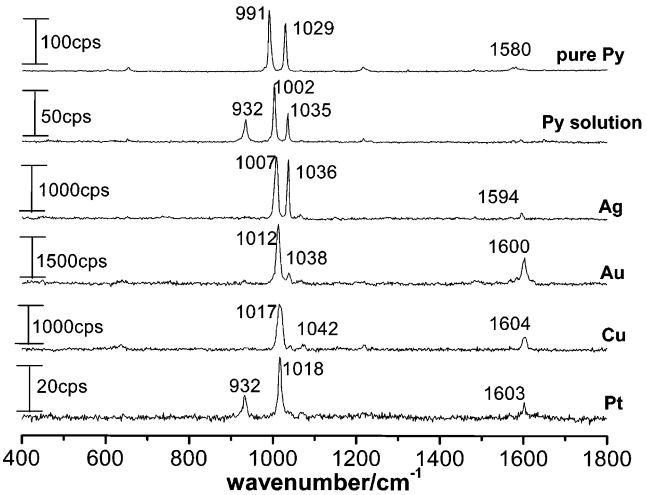

Figure 2. Normal Raman spectra of pure pyridine and pyridine aqueous solution with concentration of 0.1 M $NaClO_4$ + 0.1 M pyridine and the surface-enhanced Raman spectra of pyridine adsorbed on Ag, Au, Cu, and Pt surfaces in the solution of 0.1 M $NaClO_4$ + 0.01 M pyridine. The 932 cm^{-1} peak is from the symmetric stretching of ClO_4^- using as the supporting electrolyte. Excitation line: 632.8 nm.

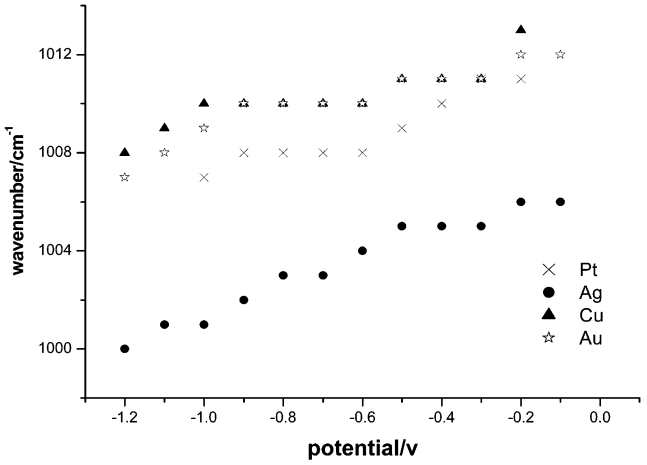

Figure 3. Frequency−potential profiles of the ν_1 mode vibration of the adsorbed pyridine on different metal surfaces as indicated in the figure.

TABLE 2: Interaction Energies and NBO Analysis of the Pyridine−Metal Complexes Calculated at the B3LYP/ 6-311+G (C, N, H)/LANL2DZ (M) Level[a]**

			NBO		
Py−metal	ΔE	ΔE + ΔZPE[b]	α: lp(N) → ns	β: lp(N) → ns	sum
Cu	12.72	12.14		20.15	20.15
Ag	4.70	4.29		9.79	9.79
Au	9.12	8.55		26.72	26.72
Cu^+	67.07	65.69	22.98	22.98	45.96
Ag^+	50.25	49.16	14.73	14.73	29.46
Au^+	76.09	74.69	45.04	45.04	90.08
Pt[c]	42.78	41.64	79.96	79.96	159.92

[a] Energy units are kilocalories per mole. [b] The zero point energy is calculated by the scaled frequencies. [c] The interaction energy refers to the energy of the singlet Pt atom.

Interaction Energy. The binding energies (ΔE_b) are summarized in Table 2. We find that ΔE_b follows the order Ag < Au < Cu < Pt < Ag^+ < Cu^+ < Au^+. The order of the stability of the complexes remains unchanged after correcting the ZPVE values to the bond energies. For the neutral complexes, the binding energy is the smallest in Py−Ag. ΔE_b increases from Au through Cu to the transition-metal atom Pt. On the other hand, in the Py−M^+ complexes, although the binding energy is still the smallest in Pt−Ag^+, the opposite order is found for Cu^+ and Au^+ such that ΔE_b (Py−Au^+) > ΔE_b (Py−Cu^+). In fact, this is not unexpected as this trend has been observed before for the carbon monoxide−ion complexes. A previous theoretical study of the binding in CO−M^+ (M^+ = Cu^+, Ag^+, and Au^+) showed that both the electrostatic interaction and the σ-donation/π-back-donation interactions play an important role.[59] The order of ΔE_b in CO−M^+ is Ag^+ < Cu^+ < Au^+. It has been shown that this trend can be understood by examining the radii of the valence s and d orbitals of the metal ions.[59] Since the electronic ground states for these three metal atoms and ions are $d^{10}s^1$ and $d^{10}s^0$, their s valence orbitals serve as the acceptor orbitals and the valence d orbitals are the donor orbitals. The radius of the 4s orbital of copper is 3.262 au, which is smaller than the radius (3.451 au) of the 5s orbital of silver, but larger than the radius (3.061 au) of the 6s orbital of gold. A small radius of the 6s orbital of gold is due to the well-known relativistic effect − the orbital contraction for the atom with high atomic mass. On the other hand, the radius of the 3d orbitals of copper is the smallest, only about 1.002 au, among the three metal atoms. The radii of the valence d orbitals of silver and gold are 1.396 and 1.618 au. As the π-back-donation strongly depends on the bond length, the π-back-donation interaction increases significantly with the decrease in the bond distance. In the case that pyridine binds to copper or gold, pyridine can come rather close to the metal to form a short and efficient σ-donation bond with the metal. This short M−N bond distance, in turn, leads to a significant π-back-donation interaction. In contrast, the 5s orbital of silver has a much larger radius, resulting in a weak π-back-donation at a longer bond length.

The NBO charges at the σ and the π spaces in Table 3 show that the ratio of the charges from π-back-donation/σ-donation for copper (1.04) is clearly larger than the ratios for silver (0.17) and gold (0.13). This suggests that the σ-donation and the π-back-donation interactions effectively occur at Py−Cu. It is interesting to note that the amount of the σ-donation charges can be larger in an ion complex than that in a neutral complex. This can be explained by the shortening of the N−M bond length by the electrostatic effect, resulting in a more effective σ-donation in the ion complex than in the corresponding neutral

TABLE 3: Amounts of NBO Charge Transfer in the σ and the π Spaces of Metal Atoms and Their Ratios of Them[a]

	metal		
species	s	p	ratio of π/σ
Py−Cu	0.023	0.024	1.04
Py−Ag	0.023	0.004	0.17
Py−Au	0.103	0.013	0.13
Py−Cu^+	0.146	0.011	0.08
Py−Ag^+	0.129	0.005	0.04
Py−Au^+	0.323	0.017	0.05
Py−Pt	0.375	0.139	0.37

[a] The variations of the populations in the complexes versus the isolated metal atom.

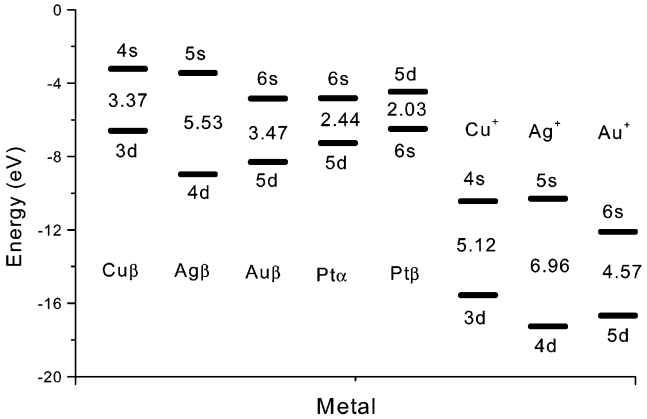

Figure 4. Occupied and unoccupied orbital levels of the free metal atoms and ions. The β spin−orbital levels for Cu, Ag, and Au are shown, and both α and β spin−orbital levels are given for Pt. For Cu^+, Ag^+, and Au^+ ions, the levels of the α and β spin−orbital are equal.

complex. The result for the Py−Pt complex shows a large ratio of 0.37 as compared to those in the Au and Ag complexes. Additionally, the amounts of the σ-donation and the π-back-donation charges are significantly large in the Py−Pt complex, leading to a very short N−Pt bond length (1.936 Å), comparable to that in Py−Cu^+ (1.932 Å). The N−Pt bond length is significantly smaller than the N−Au bond distances in Py−Au (2.391 Å) and Py−Au^+ (2.056 Å), although Pt (atomic radius = 1.39 Å) and Au (atomic radius = 1.46 Å) are neighbors in the periodic table.

The orbital energies and their occupations are also important for understanding the bonding mechanism of the metal−pyridine complexes. The interaction of the filled lone pair of electrons on nitrogen with the filled metal d_{z^2} (d_σ) or s atomic orbitals leads to the σ-repulsion. In general, sd_σ mixing in the metal center shifts the electron density away from the N−M bond axis to the *xy* plane, decreasing the σ-repulsion and allowing for a stronger metal−ligand σ-donation. The degree of the $s-d_\sigma$ mixing depends on the $s-d_\sigma$ energy gap. The energy gaps of the metal atoms and ions given in Figure 4 show that the Pt atom with the smallest energy gap about 2.03−2.44 eV forms the strongest bond among the neutral complexes, while the Ag ion with the largest energy gap about 6.96 eV forms the weakest bond among the ion complexes. The strength of the interaction of pyridine with Cu, Au, and their ions falls between silver and platinum. Figure 4 also shows that the energy levels of the acceptor orbitals are significantly lower for metal ions, in agreement with previous studies. In the next section, we show that the force constant of the N−Pt bond is the largest and the force constant of the N−Ag bond is the smallest. The order of the force constants of the other bonds is Au < Cu < Ag^+ < Cu^+ < Au^+. The σ-donation interaction energies of the lone

TABLE 4: Comparisons of the Scaled Frequencies of the Vibrations for the Pyridine−Metal and the Pyridine−Metal Ion Complexes

modes	expt[a]	pyridine	Py−Cu	Py−Ag	Py−Au	Py−Cu$^+$	Py−Ag$^+$	Py−Au$^+$	Py−Pt
A_1									
υ_2	3094.2	3088.7	3094.7	3092.8	3095.8	3112.2	3110.5	3123.6	3132.1
υ_{13}	3072.8	3065.4	3074.8	3071.3	3078.4	3098.3	3095.5	3107.9	3098.8
υ_{20a}	3030.1	3046.0	3063.2	3055.3	3068.9	3089.7	3087.7	3092.6	3078.4
υ_{8a}	1583.9	1592.4	1605.7	1600.0	1600.2	1614.7	1609.4	1606.2	1604.0
υ_{19a}	1483.4	1482.0	1482.8	1483.4	1479.9	1490.4	1488.9	1482.9	1468.4
υ_{9a}	1218.0	1218.2	1211.5	1215.4	1210.0	1221.6	1222.4	1217.6	1195.3
υ_{18a}	1071.9	1072.4	1069.0	1071.1	1070.1	1074.6	1071.4	1073.9	1070.5
υ_{12}	1031.7	1027.0	1030.4	1027.1	1024.9	1046.7	1035.0	1042.1	1053.1
υ_1	991.4	991.3	1004.2	999.0	1002.6	1015.8	1010.4	1015.7	1009.4
υ_{6a}	601.4	605.1	625.4	615.9	620.6	656.4	637.1	659.0	672.5
υ_{NM}			162.0	86.4	106.8	261.1	184.6	225.5	261.5
A_2									
υ_{17a}	966	983.8	980.2	981.5	983.2	986.8	986.6	988.6	970.8
υ_{10a}	871	877.4	875.5	877.1	875.7	875.1	875.1	862.5	851.3
υ_{16a}	373	374.5	366.6	371.1	379.2	384.2	384.9	392.2	397.4
B_1									
υ_5	1007	994.8	995.5	996.5	999.8	1019.9	1020.9	1022.1	985.8
υ_{10b}	936.6	939.4	941.6	940.0	943.5	953.0	950.5	955.3	924.0
υ_4	744.0	745.2	743.2	744.1	747.1	760.4	756.4	760.5	745.7
υ_{11}	700.3	702.8	695.2	699.3	697.3	695.0	696.1	685.8	681.4
υ_{16b}	403.3	410.3	414.9	415.1	416.7	421.4	417.5	427.7	441.5
υ_ω			36.3	57.7	64.1	113.3	86.3	121.4	125.4
B_2									
υ_{20b}	3086.9	3081.1	3088.5	3086.0	3090.0	3108.6	3106.5	3122.2	3131.2
υ_{7b}	3042.4	3043.7	3064.2	3054.8	3073.0	3095.1	3091.4	3104.1	3091.2
υ_{8b}	1580.5	1586.9	1583.2	1587.3	1586.5	1579.1	1581.1	1576.3	1561.8
υ_{19b}	1441.9	1442.0	1447.4	1446.2	1448.2	1454.8	1453.4	1458.1	1446.4
υ_{14}	1362.3	1357.9	1354.8	1357.1	1351.8	1366.9	1366.6	1361.5	1340.0
υ_3	1227	1259.7	1266.9	1265.9	1268.1	1268.1	1267.2	1265.9	1251.1
υ_{15}	1143.3	1148.3	1153.2	1151.4	1152.8	1168.6	1167.0	1169.8	1153.1
υ_{18b}	1079	1056.0	1064.6	1061.9	1064.2	1079.1	1077.9	1083.0	1066.0
υ_{6b}	652	656.8	652.2	653.9	651.4	648.4	648.7	642.6	645.8
υ_σ			113.6	81.5	107.5	167.2	137.4	193.3	211.9

[a] The experimental data are extracted from refs 49, 62, 67.

pair of electrons on the nitrogen atom with the d_σ or s orbitals of the metal atoms (ions) are shown in Table 2. For the neutral metal atoms such as Cu, Ag, and Au, the σ-donation interaction only takes place in the β spin space due to the strong σ-repulsion in the α spin space. The σ-donation interactions are stronger in the Cu and the Au complexes than in the Ag complex. Because of the electronic configurations of $d^{10}s^0$ in the coinage metal ions, the σ-donation interaction can take place both in the α and the β spin spaces. The amount of the σ-donation is much larger in Py−M$^+$ than that in the corresponding Py−M complex. NBO analysis shows that the Py−Pt complex has the strongest σ-donation interaction due to the low occupations at the s−d_σ orbitals.

Normal-Mode Analysis. For the pyridine molecule, there are a number of studies analyzing the frequencies and the assignments of the vibrational modes.[18,19,49−51,58,60,61] The vibrational analysis of the pyridine experimental spectra as well as the predicted frequencies for the free pyridine molecule and its metal complexes at the B3LYP/6-311+G**/LANL2DZ level are summarized in the Table 4. These predicted frequencies have been scaled by using the SQMF procedure as described above. For the free pyridine molecule, the mean deviation between the experimental frequencies and our DFT frequencies after scaling is 2.4 cm^{-1}, which is considerably smaller than the mean deviation values of 8 cm^{-1} of Dkhissi et al., who used a larger basis set of 6-311++G(2d,2p) but without using the SQMF procedure.[19]

A. Free Pyridine. As is shown in Table 4, our SQM scaled B3LYP frequencies are very close to the experimental spectra for the free pyridine molecule. In particular, our calculated υ_1 (991.3 cm^{-1}) is identical to the experimental data (991.4 cm^{-1}).[49,62,67] But it is worth noting that there still exist some controversies. First, there are different assignments for the total-symmetric vibrational modes υ_{13} and υ_{20a} belonging to the C−H stretching vibrations. Wiberg et al. assigned the observed frequencies of 3072.8 and 3030.1 cm^{-1} with a 0.24 cm^{-1} resolution to these two modes, respectively;[49,62] on the other hand Castellucci et al. obtained 3065 and 3042 cm^{-1} for these two modes, respectively.[50,63] Our calculated frequencies after scaling are 3065.4 and 3046.0 cm^{-1} for the two modes, respectively, which is in a better agreement with the values of Castellucci et al.[63]

Second, the out-of-plane vibrational mode, υ_{17a} belongs to the highest frequency of the A_2 symmetry in pyridine. According to the experiments[64,65] and Pulay's calculation[51] the band at 980 cm^{-1} was attributed to the mode. But Wiberg et al. quoted the band at 966 cm^{-1} to this mode.[49] Our calculated value of 983.8 cm^{-1} supports the former assignment. Among the A_2 modes, our calculated value of the υ_{10a} mode is 877.4 cm^{-1}, which is in better agreement with a recent gas-phase Raman spectrum appearing at 875 cm^{-1} [53] than the previous assignment of Wiberg et al. of 871 cm^{-1} for the υ_{10a} mode.

Third, as pointed out before, the theoretical scaled frequency of the υ_5 mode is always lower than the experimental value of 1007 cm^{-1}.[64] Our calculated value is not an exception, which is about 12 cm^{-1} lower than the experimental one. Klots' Raman spectrum using a high-quality sample showed the lack of any notable peak near 1007 cm^{-1}.[53] He suggested that the earlier experimental frequency be possibly related to an impurity. In his Raman spectrum, a band at 997.4 cm^{-1} was assigned to the

difference frequency of two modes with the A_1 symmetry. On the basis of the present calculation, we recommend assigning this band to the υ_5 mode.

Fourth, among the B_2 modes, there have been debates concerning the frequencies of the υ_3 mode. The frequency of the υ_3 mode was observed at 1227 cm^{-1} in the earlier spectra[64,65] and 1228 cm^{-1} in a recent Raman vapor spectrum.[53] Indeed, as pointed out in a recent paper,[19] the experimental data deserves a closer attention. On the basis of the HF−SQM procedure, the predicted frequency was either about 10−13 cm^{-1} higher with small basis sets[49,50,61] or about 21 cm^{-1} lower with large basis sets than the experimental data.[18,66] Some recent DFT calculations predicted the υ_3 frequency that is significantly higher than the experimental value.[19,58] The unscaled frequencies of 1306 and 1283 cm^{-1} were given by the B3LYP method with the cc-pVDZ and cc-pVTZ basis sets, respectively.[19] If a scaled factor of 0.975 is applied to these two frequencies, the resultant numbers of 1273 and 1251 cm^{-1} are still remarkably larger than the experimental value of 1227 cm^{-1}. We obtain 1259.7 cm^{-1} for the υ_3 mode. Thus, all theoretical calculations lead to the conclusion that the fundamental frequency of the υ_3 mode should be higher than the currently assigned value. Indeed, in a recent Raman spectrum, one peak at 1260 cm^{-1} was observed,[53] which could be assigned to the fundamental frequency of the υ_3 mode.

There are controversies in assigning the υ_{18b} mode of the B_2 symmetry.[67] The present calculation leads to a frequency at 1056.0 cm^{-1}, which has a deviation of about 23 cm^{-1} from the assigned frequency at 1079 cm^{-1} in the experiment of Wiberg et al. On the other hand, our result supports Pulay's assignment of a band at 1052 cm^{-1} at the Raman spectrum to the υ_{18b} mode.[50]

B. Pyridine−Metal. The N−M stretching vibrations belong to the low-frequency modes. The results in Table 4 show that the vibrational frequency of the N−M(metal) stretching is the largest for N−Pt and the smallest for N−Ag. Considering the differences in the reduced masses, the order of the vibrational frequencies υ_{N-M} is in line with that of the bond energies ΔE_b except for the Py−Pt complex. Although the bond energy for the Py−Pt complex is relatively smaller as compared to those of the positively charged complexes, the force constant (about 3.06×10^5 dyn/cm) of the N−Pt bond is the largest. This can be understood by the fact that the N−Pt bond is the strongest covalent bond among these complexes, having the largest σ-donation/π-back-donation; on the contrary in the ion complexes, the electrostatic interaction contributes a large amount to the bond energy. For pyridine adsorbed on these metal surfaces, the N−M vibrational frequencies have been reported by Pettigner[68] and Creighton,[7a,70] respectively. In the surface Raman spectrum of pyridine adsorbed on the silver surface, the bands observed at 173 and 252 cm^{-1} were attributed to the pyridine−silver vibrations.[68] A weak band with a lower frequency of 65 cm^{-1} was also observed.[68] If Pettinger's assignment is corrected, the assigned frequencies of 173 and 252 cm^{-1} are clearly larger than our calculated value (86 cm^{-1}) for the pyridine−silver complex. In addition, a comparison of the bond energy (4.7 kcal/mol for Py−Ag) with the adsorption heat of about 11.8 kcal/mol for pyridine adsorbed on the Ag(111) surface from a recent temperature-programmed desorption spectrum indicates that the interaction between pyridine and silver is possibly stronger on the solid surface than that in the Py−Ag complex.[69] For pyridine adsorbed on the copper surface, a band observed at 244 cm^{-1} is attributed to the N−Cu stretching vibration,[70] while for pyridine adsorbed on the gold surface a band at 260 cm^{-1} is assigned to the N−Au stretching vibration.[7a] For pyridine adsorbed on the Pt(111) surface, a band at 290 cm^{-1} in the electron energy-loss spectrum is thought to be from the N−Pt vibration. The activation energy for the pyridine desorption from Pt(111) at the low coverage is 21.8 kcal/mol, while it drops to 15.0 kcal/mol at the saturation coverage due to the repulsive adsorbate−adsorbate interaction.[71] At the Cu(110) surface, the desorption energy decreases from 22.4 kcal/mol at the low coverage to 18.7 kcal/mol at the monolayer.[5f] Although the reported experimental adsorption energies do not match the calculated binding energies in the Py−M complexes, agreement is reached in that the N−Ag bond is the weakest among this series. In the literature, there is still no complete and clear assignment of the N−M stretching modes at the metal surfaces because all the N−M and the M−M vibrational modes have a very weak spectral signal and a small difference in frequency.

As compared to the vibrational frequencies of the free pyridine molecule, the upward or downward shifts of these frequencies reveal the bonding nature of the interaction between pyridine and the metals. As is seen in Table 4, there is a blueshift for the five high-frequency modes (υ_2, υ_{13}, υ_{20a}, υ_{20b}, and υ_{7b}) of the C−H stretching vibrations in all the pyridine−metal complexes. The blueshifts are larger in $Py-M^+$ due to the strong electrostatic interaction and in Py−Pt due to the strong σ/π dative interactions than those in Py−M (M = Cu, Ag, Au). The C−H in-plane bending vibrations (υ_{19a} and υ_{9a} of the A_1 symmetry, υ_3, υ_{14}, and υ_{19b} of the B_2 symmetry) generally encounter a smaller change as compared to the C−H stretching modes. The shifts of the C−H in-plane bending can be upward or downward. Except υ_{19b} of Py−Pt, which has a small blueshift, sizable redshifts are seen in Py−Pt for all the other C−H in-plane bending modes.

The υ_1 mode belongs purely to the stretching mode from the combination of the C−N and C−C stretching vibrations. In the free pyridine molecule, the υ_1 mode strongly couples with the stretching and bending motions of the heavy atoms. According to the present PEDs from the normal-mode analysis, the υ_1 mode contains 38% the trigonal symmetric deformation (S_8) and 62% the ring backbone stretchings ($S_1 + S_2 + S_3$ in Table 5). In some previous normal-mode analyses, the S_8 coordinate contribution to the υ_1 mode was found to be about 35% at the HF/3-21G level,[61] 31% at the HF/6-31++G** level,[18] and 43% at the B3LYP/6-31++G** level for the free pyridine molecule.[19] Furthermore, our PED results show that the S_8 coordinate contribution to the υ_1 mode is sensitive to the interaction between pyridine and the metal atoms or ions, and the PED value decreases with the increase in the strengths of the N−M bonds. In the neutral complexes, the PEDs for the S_8 coordinate range from 10% to 33%, where Py−Pt has the smallest PED of 10% due to the strongest Pt−N bond and Py−Ag has the largest PED of 33% due to the weakest Ag−N bond. On the other hand, the S_8 contribution to υ_1 decreases to less than 10% in $Py-M^+$, where the contribution of the S_8 coordinate is almost negligible in $Py-Cu^+$.

On the contrary, the PED value of the S_8 contribution to the υ_{12} mode seems to increase with the strength of the N−M bond. In the neutral complexes, the PEDs increase from 54% for Py−Ag to 69% for Py−Cu, while in the ion complexes the contribution of the S_8 coordinate to the υ_{12} mode is higher than 89%, with PEDs in $Py-Cu^+$ coming almost exclusively from the contribution of the S_8 coordinate. Interestingly, the PED of S_8 to υ_{12} in Py−Pt is the smallest among this series, even though Pt−N is the strongest dative bonding. Experimentally, an intense 1035 cm^{-1} band (υ_{12}) can be observed on the Ag electrode. Its

TABLE 5: Comparison of the Potential Energy Distributions (PEDs) of the Ring Breathing Mode, the Ring Deformation Modes, and the N−M Stretching of Pyridine and Its Complexes, Calculated at the B3LYP/6-311+G(C,N,H)/LANL2DZ(M) Level[a]**

species	υ_{8a}	υ_{9a}	υ_{18a}	υ_{12}	υ_{1}	υ_{6a}	υ_{NM}
Py	$S_2(43)$, $S_3(14)$, $S_{11}(13)$, $S_1(11)$, $S_8(11)$, $S_9(8)$	$S_{10}(38)$, $S_1(20)$, $S_{11}(20)$, $S_2(9)$	$S_{11}(33)$, $S_3(22)$, $S_1(19)$, $S_8(13)$	$S_8(47)$, $S_3(31)$, $S_2(14)$	$S_8(38)$, $S_1(32)$, $S_2(19)$, $S_3(11)$	$S_9(95)$	
Py−Cu	$S_2(44)$, $S_3(13)$, $S_{10}(12)$, $S_1(11)$, $S_{11}(11)$, $S_9(9)$	$S_{10}(38)$, $S_{11}(23)$, $S_1(16)$, $S_2(11)$	$S_{11}(29)$, $S_3(25)$, $S_1(24)$, $S_8(10)$	$S_8(69)$, $S_3(18)$, $S_2(6)$, $S_7(1)$	$S_1(32)$, $S_2(24)$, $S_3(22)$ $S_8(18)$, $S_7(1)$	$S_9(90)$, $S_7(6)$	$S_7(92)$, $S_9(5)$
Py−Ag	$S_2(44)$, $S_3(13)$, $S_{10}(12)$, $S_1(12)$, $S_{11}(12)$, $S_9(8)$	$S_{10}(38)$, $S_{11}(21)$, $S_1(18)$, $S_2(9)$	$S_{11}(31)$, $S_3(23)$, $S_1(22)$, $S_8(11)$	$S_8(54)$, $S_3(27)$, $S_2(11)$	$S_8(33)$, $S_1(31)$, $S_2(20)$ $S_3(15)$, $S_7(2)$	$S_9(92)$, $S_7(2)$	$S_7(97)$, $S_9(3)$
Py−Au	$S_2(44)$, $S_3(13)$, $S_{11}(12)$, $S_{10}(11)$, $S_1(11)$, $S_9(9)$	$S_{10}(39)$, $S_{11}(22)$, $S_1(16)$, $S_2(10)$	$S_{11}(30)$, $S_1(25)$, $S_3(23)$	$S_8(58)$, $S_3(24)$, $S_2(11)$	$S_1(30)$, $S_8(29)$, $S_2(20)$ $S_3(18)$, $S_7(2)$	$S_9(91)$, $S_7(4)$	$S_7(95)$, $S_9(4)$
$Py-Cu^+$	$S_2(44)$, $S_{10}(13)$, $S_1(12)$, $S_3(11)$, $S_{11}(10)$, $S_9(9)$	$S_{10}(36)$, $S_{11}(27)$, $S_1(14)$, $S_2(13)$	$S_1(34)$, $S_{11}(25)$, $S_3(24)$, $S_7(4)$	$S_8(93)$, $S_3(1)$, $S_7(5)$	$S_3(41)$, $S_2(28)$, $S_1(21)$, $S_8(1)$, $S_7(2)$	$S_9(78)$, $S_7(14)$	$S_7(75)$, $S_9(15)$
$Py-Ag^+$	$S_2(45)$, $S_{10}(13)$, $S_3(12)$, $S_1(11)$, $S_{11}(10)$, $S_9(9)$	$S_{10}(36)$, $S_{11}(26)$, $S_1(15)$, $S_2(12)$	$S_1(29)$, $S_3(28)$, $S_{11}(27)$, $S_8(3)$, $S_7(1)$	$S_8(89)$, $S_3(5)$, $S_7(2)$	$S_3(34)$, $S_1(28)$, $S_2(27)$, $S_8(5)$, $S_7(3)$	$S_9(85)$, $S_7(9)$	$S_7(86)$, $S_9(8)$
$Py-Au^+$	$S_2(46)$, $S_{10}(14)$, $S_3(13)$, $S_{11}(11)$, $S_1(10)$, $S_9(9)$	$S_{10}(36)$, $S_{11}(27)$, $S_1(13)$, $S_2(13)$	$S_1(36)$, $S_{11}(24)$, $S_3(22)$, $S_8(1)$, $S_7(5)$	$S_8(89)$, $S_3(6)$, $S_7(6)$	$S_3(41)$, $S_2(26)$, $S_1(21)$, $S_8(4)$, $S_7(2)$	$S_9(79)$, $S_7(14)$	$S_7(72)$, $S_9(14)$
Py−Pt	$S_2(46)$, $S_3(14)$, $S_{11}(13)$, $S_{10}(10)$, $S_1(9)$, $S_9(9)$	$S_{10}(36)$, $S_{11}(30)$, $S_2(14)$, $S_1(9)$	$S_8(31)$, $S_1(28)$, $S_7(15)$, $S_{11}(10)$, $S_3(10)$, $S_{10}(6)$	$S_8(50)$, $S_3(24)$, $S_{11}(13)$, $S_7(2)$	$S_3(31)$, $S_1(27)$, $S_2(24)$, $S_8(10)$, $S_7(3)$	$S_9(73)$, $S_7(20)$	$S_7(61)$, $S_9(20)$

[a] The symmetric coordinates are defined as follows. S_1, C−N symmetric stretching: $(2)^{-1/2}[r(N-C_2) + r(N-C_6)]$. S_2, C−C symmetric stretching: $(2)^{-1/2}[r(C_2-C_3) + r(C_5-C_6)]$. S_3, C−C symmetric stretching: $(2)^{-1/2}[r(C_3-C_4) + r(C_5-C_4)]$. S_4, C−H symmetric stretching: $(2)^{-1/2}[r(C_2-H_7) + r(C_6-H_{11})]$. S_5, C−H symmetric stretching: $(2)^{-1/2}[r(C_3-H_8) + r(C_5-H_{10})]$. S_6, C−H stretching: $r(C_4-H_9)$. S_7, N−M stretching: r(N−M). S_8, symmetric ring deformation: $(6)^{-1/2}[a(C_2-N_1-C_6) - a(N_1-C_2-C_3) - a(N_1-C_6-C_5) + a(C_2-C_3-C_4) + a(C_6-C_5-C_4) - a(C_3-C_4-C_5)]$. S_9, asymmetric ring deformation: $(12)^{-1/2}[2a(C_2-N_1-C_6) - a(N_1-C_2-C_3) - a(N_1-C_6-C_5) - a(C_2-C_3-C_4) - a(C_6-C_5-C_4) + 2a(C_3-C_4-C_5)]$. S_{10}, C−H in-plane bending: $(2)^{-1/2}[\beta(C_3-H_7) - \beta(C_5-H_{11})]$. S_{11}, C−H in-plane bending: $(2)^{-1/2}[\beta(C_2-H_7) - \beta(C_6-H_{11})]$. Here r and a denote the bond distance and bond angle, respectively. β denotes the in-plane bending angle.

Raman intensity significantly decreases from silver to gold, copper, and platinum, as observed above.

In the literature, the different behaviors of υ_1 and υ_{12} are attributed to the different surfaces used, resulting in the difference in the cooperative contribution from the electromagnetic (EM) and the chemical enhancements.[7,8] Considering that the adsorption orientation of pyridine is the same on these metal surfaces, the EM enhancement should give an approximately equal enhancement factor for both the υ_1 and the υ_{12} modes on all surfaces. Therefore, it could be possible that the difference in the enhancement of these two modes is partially due to the difference in the chemisorption on these metal surfaces. In the present work, the PEDs of both modes are found to rely strongly on the properties of the pyridine N−metal bonds. It is generally accepted that the larger the force constant of the N−metal bond, the smaller the PED of the ring symmetric stretching coordinates in the υ_{12} mode, and the larger the PED of the S_8 coordinate in the υ_{12} mode. (Py−Pt is an exception, possibly due to a different bonding mechanism). This will also influence the displacement between the minima of the potential surfaces at the excited charge-transfer states and the ground state, resulting in the different extent of chemical enhancement for these two modes.[8] Therefore, it is very likely that the difference in the nature of Py−M bonding gives rise to the difference between υ_1 and υ_{12} and the difference of the two modes among different metals.

Now let us consider the υ_{18a} mode. The PEDs of the mode in the free pyridine molecule are about 33% from the in-plane bending of the C−H bonds neighboring to nitrogen atom (S_{11}), 22% from the stretching of the two C−C bonds (S_3), 19% from the stretching of the C−N bonds (S_1), and 13% from the symmetric ring deformation (S_8). In the neutral complexes of Cu, Ag, and Au, the PEDs from the C−N stretchings (S_1) increase while the PEDs of the in-plane C−H bending (S_{11}) decrease. However, for Py−Pt, the PED of the S_8 coordinate increases to 31% and the PED of the in-plane C−H bending (S_{11}) decreases to 11% due to the different bonding mechanism. In the three ion complexes, the PEDs of the S_8 coordinate are all less than 3%, as listed in Table 5.

According to the PED values, it can be seen that the asymmetric ring deformation (S_9) contributes dominantly to the υ_{6a} mode with the A_1 symmetry. The degree of the blueshifts of this mode depends on the strength of the N−M bond. Furthermore, the PED of the N−M stretching (S_7) increases in the normal mode, indicating that there is a strong coupling between the S_9 coordinate and the N−M stretching. This will be further discussed later from the coupling between the different vibrational modes.

For the υ_{8a} mode, the results in Table 4 show that there is a blueshift between 7.6 (in Py−Ag) and 22.3 cm^{-1} (in $Py-Cu^+$) upon interaction with the metal atoms (ions). This can be explained by the increase in the force constants of the two parallel C−C bonds from 6.57×10^5 dyn/cm for the free pyridine molecule through 6.76×10^5 dyn/cm for the neutral complexes of the coinage metals to no less than 6.82×10^5 dyn/cm for the complexes of Pt and the charged ions. The PEDs for υ_{8a} shown in Table 5 only experience a small change upon interaction with the metals. The PED from the symmetric stretch of the two parallel C−C bonds (S_2) increases slightly by 1% in the neutral complexes of Cu, Ag, and Au, and by 1−3% in the complexes of Pt and the charged ions.

For the ring backbone modes with the B_2 symmetry, the frequencies of υ_{6b} and υ_{8b} modes redshift, while the frequencies of the υ_{15} and υ_{18b} modes blueshift. The degree of the frequency shifts has a complicated relationship with the bonding interaction between pyridine and the metal atoms (ions).

Coupling of Vibration Modes. As shown in Table 5, the changes of the PEDs of the S_8 coordinate in the υ_1 and υ_{12} modes strongly depend on the strengths and the bonding properties between pyridine and the metal atoms (ions); however, the vibrational frequency and the PEDs of the υ_{18a} modes are not very sensitive to the strength of the N−M bond. In the literature, the frequency shift of the υ_1 mode was used to measure the interaction between pyridine and a metal atom (ion) in the pyridine hydrogen-bonded complexes and for pyridine adsorbed on surfaces.[14,21] Moreover, our calculations show that the frequency shift of the υ_{6a} mode is closely associated with the change of the N−M bond, which can be another strong indicator of the bonding strength between pyridine and the metal atoms or ions. A coupled oscillator method can be utilized to describe the couplings between two or more vibrational modes. The model Hamiltonian of the coupled vibrational modes is similar to the Hamiltonian used in our normal-mode analysis. The

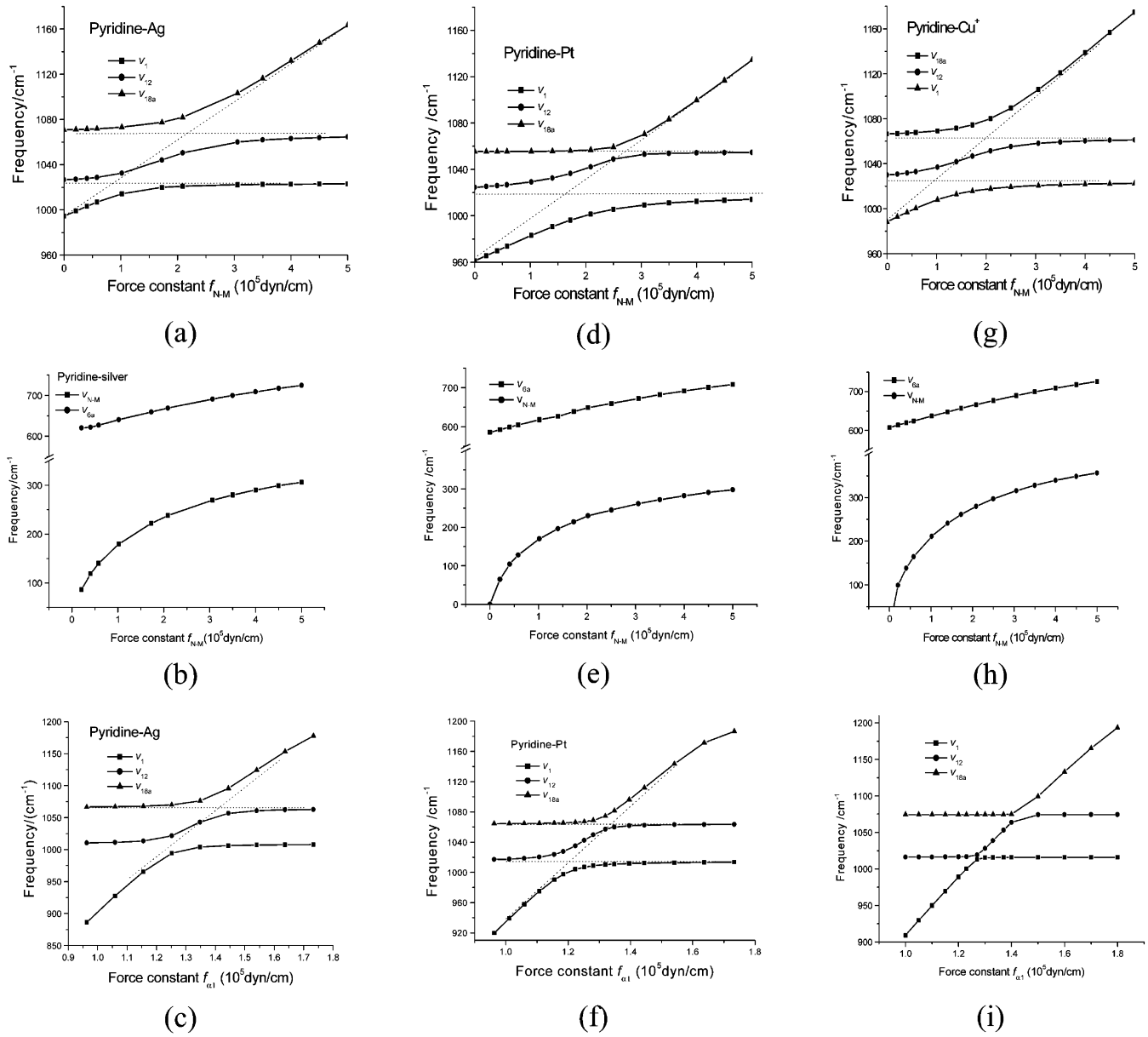

Figure 5. Coupling of the vibrational modes with the force constants of the N−M stretch or the trigonal symmetric deformation. (a), (d), and (g) Coupling of the υ_1, υ_{12} and υ_{18a} modes with the N−M stretch. (b), (e), and (h) Coupling of the υ_{6a} mode with the force constant of the N−M stretch. (c), (f), and (i) Coupling of the υ_1, υ_{12} and υ_{18a} modes with the force constant of the trigonal symmetric deformation.

frequency shifts of the υ_1, υ_{12}, υ_{6a}, and υ_{18a} modes are investigated by increasing the force constants of the N−M stretching and the ring deformation, respectively. In the present work, the coupling nondiagonal elements of the force constant matrix are kept in the DFT−SQM values.

Mizutani and Ushioda suggested that there are two types of bonding that result in distinct shift patterns of the normal-mode frequencies upon adsorption or coordination.[14] The metal ion-type bonding is characterized by a strong pyridine−substrate bond, which results in large frequency shifts; on the other hand, the halogen-type bonding causes a comparatively small frequency shift due to the weaker bonding. Therefore, the ion Py−M^+ (M^+ = Cu^+, Ag^+, Au^+) complexes fall into the metal ion-type and the Py−M (M = Cu, Ag, Au) complexes belong to the halogen-type. As is shown in the present work, however, a N−M bond like Py−Pt can be stronger than that in Py−M^+. In this case, how to understand the frequency shift of the relevant modes is a question to be answered in this section. For this purpose, we analyze the frequency shifts due to the couplings of the vibrational modes in three types of bonding systems, e.g., Py−Ag, Py−Pt, and Py−Cu^+. The force constants of the N−M stretching (S_7) and the ring deformation (S_8) are varied in a wide range from 0.0 to 5.0 × 10^5 dyn/cm for S_7 and from 1.0 to 1.8 × 10^5 dyn/cm for S_8.

A. Py−Ag. The bonding in the Py−Ag complex belongs to the halogen-type, which has a weak N−M bond and has small changes in the geometric and the electronic structures of pyridine. Figure 5a,b shows dependence of the vibrational frequencies of υ_1, υ_{12}, υ_{6a}, and υ_{18a} on the force constant of the N−Ag bond. As is seen from Figure 5a, υ_1, υ_{12}, and υ_{18a} couple with each other. When the force constant of the N−Ag bond approaches zero, υ_1, υ_{12}, and υ_{18a} approach 994.4, 1026.6, and 1070.8 cm^{-1}, respectively, which correspond to the respective frequencies (991.3 (υ_1), 1027.0 (υ_{12}), and 1072.4 (υ_{18a}) cm^{-1}) of the free pyridine molecule. With the increase in the force constant of the N−Ag bond, υ_1 and υ_{12} reach a limit value of 1022.5 and 1063 cm^{-1}, respectively. Thus the up limit of υ_1 corresponds to υ_{12} in the free pyridine molecule, while that of

υ_{12} corresponds to υ_{18a} in the free pyridine molecule. It is clear that the coupling between different modes significantly change the dependence of the vibrational frequencies on the force constant of the N−Ag bond. If there were no such a coupling, the frequency shift of the υ_1 mode would not be proportional to the strength of N−M bond and it also would not reflect the strength of the N−M bond. As is seen from Figure 5a, the frequency of the υ_{18a} mode blueshifts sharply with the increase in the force constant of the N−M bond owing to the strong coupling.

A comparison of the frequency shift of the υ_{6a} mode with that of the N−M stretching shown in Figure 5b indicates that the υ_{6a} mode almost has a linear frequency dependence on the force constant of the N−M bond. The trend in the frequency shift is fairly appropriate to reflect the strength of the N−M bond between pyridine and an electron acceptor.

Although the shapes of the curves in Figure 5c are fairly similar to those in Figure 5a, these curves reflect the dependence of the coupling of three vibrational modes (i.e., υ_1, υ_{12}, and υ_{18a}) on the force constant of the S_8 coordinate. With the increase in the force constant of the S_8 coordinate, the coupling enhances and the PED value of the S_8 coordinate in the υ_1 mode decreases. When the change of the force constant of the S_8 coordinate is beyond the coupling region, the frequency of the υ_1 mode approaches the frequency of the υ_{12} mode in the case of the decoupling, arising from the contribution of the stretching motions of the pyridine ring.

B. Py−Pt. The Py−Pt complex has a strong N−Pt bond and undergoes large structural changes of the pyridine ring. The structural parameters in the complex are similar to those in the Py−M^+ complexes. The influence of the force constants of the internal modes on the coupling can be seen from Figure 5d−f. When the force constant of the N−Pt bond is taken as zero, the frequencies of the υ_1, υ_{12}, and υ_{18a} modes decrease to 961.1, 1024.6, and 1055.4 cm^{-1}, respectively. In this case, the PEDs are $S_1(59)$, $S_2(16)$, and $S_8(19)$ for the υ_1 mode and $S_2(8)$, $S_3(20)$, and $S_8(66)$ for the υ_{12} mode, which clearly shows that the C−N stretching motion makes the largest contribution to the υ_1 mode, while the ring deformation (S_8) contributes the most to the υ_{12} mode. Increasing the force constant of the N−Pt bond results in the upshift of the frequencies of the υ_1 and υ_{12} modes, while the vibrational frequency of the υ_{18a} mode almost remains constant until the force constant of the N−Pt bond increases to 2.0×10^5 dyn/cm (see Figure 5d). With the increase in the force constant of the N−Pt bond from 2.0×10^5 to 5.0×10^5 dyn/cm, the frequency of the υ_{18a} mode increases sharply, while the frequencies of the υ_1 and υ_{12} modes approach the limit values of 1024.6 and 1055.4 cm^{-1}. A comparison of the frequency upshift of the υ_1 mode in Py−Pt and Py−Ag indicates that the coupling between the υ_1 mode and the N−M bond increases and the coupling region becomes wider in the Py−Pt.

The frequency of the υ_{6a} mode varies linearly with the force constant of the N−Pt bond, as is shown in Figure 5e. This is true even at the large force constant. The linear dependence originates from the coupling between the S_9 coordinate and the N−Pt stretching. The PEDs also show that the S_9 coordinate mainly contributes to the υ_{6a}, υ_{8a}, and the N−Pt stretching modes. As seen in Table 5 for the PEDs of the υ_{6a} mode, a decrease in the S_9 contribution is accompanied by an increase in the mixing with the N−Pt stretch motion (S_7) with the increase of the strength of the N−Pt bond.

Figure 5f shows the variation of the frequencies for the υ_1, υ_{12}, and υ_{18a} modes with the force constant of the S_8 coordinate. If there is no coupling between the υ_1 and υ_{12} modes, the PEDs

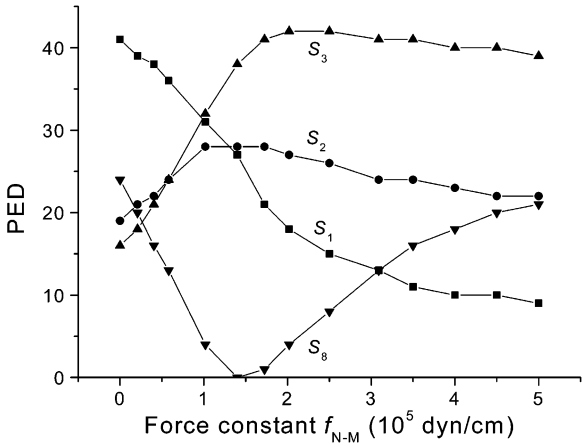

Figure 6. Dependence of the PED of the υ_1 mode on the force constant of the N−M stretching mode in the Py−Cu^+ complex.

are $S_7(8)$ and $S_8(85)$ for the υ_1 mode and $S_1(23)$, $S_2(25)$, $S_3(39)$, and $S_7(9)$ for the υ_{12} mode. Increasing the force constant of the S_8 coordinate to 1.252×10^5 dyn/cm, the coupling enhances and the frequencies of these two modes increase, while the frequency of the υ_{18a} mode almost remains unchanged. With the further increase in the S_8 force constant, the frequency of the υ_{18a} mode quickly increases, and the frequencies of the υ_1 and υ_{12} modes gradually approach the limit values. In the Py−Pt since the scaled force constant (1.296×10^5 dyn/cm) of the S_8 coordinate is larger than the turning point 1.252×10^5 dyn/cm, the coupling results in a small PED value of the S_8 coordinate in the υ_1 mode and large PED values for the υ_{12} and υ_{18a} modes (see Table 5).

C. Py−Cu^+. The bonding in the Py−Cu^+ belongs to the metal ion-type, which has a stronger N−Cu^+ bond and has larger changes in the geometric and the electronic structures of pyridine as compared with its neutral complex. Parts g and h of Figure 5 show how the frequencies of the related modes vary with the force constant of the N−Cu^+ bond. The results in Figure 5g show that the frequencies of the υ_1, υ_{12}, and υ_{18a} modes approach the corresponding values in the free pyridine if the force constant of the N−M bond is taken as zero. However, the PEDs are very different from those in the free pyridine (cf. Figure 6 and Table 5). By increasing the force constant of the N−M bond, the frequencies of these modes increase due to the coupling. From our normal-mode analysis, the PEDs for the υ_1 mode are sensitive to the change of the force constant of the N−M bond. A detailed analysis of the dependence of the PEDs for the υ_1 mode on the force constant of the N−M stretching mode is shown in Figure 6. The PED of the two parallel C−C bonds (S_2) approaches a maximum at the force constant around 1.4×10^5 dyn/cm, while the PED of the S_8 coordinate has a minimum at the same location. The trends of the PED changes for the C−N stretching (S_1) and the other C−C stretching (S_3) for the υ_1 mode are opposite as found in Figure 6. For Py−Cu^+, the υ_1 mode almost purely belongs to the stretching motion of the ring backbone of pyridine. This can also be found in Table 5 for Py−Ag^+ and Py−Au^+ ion complexes. We believe that the electrostatic effect leads to the decoupling between the S_8 coordinate and the backbone stretching motion of pyridine ring.

Again, we find the frequency of the υ_{6a} mode (Figure 5h) varies linearly with the force constant of the N−M bond. The result supports our suggestion that the frequency shift of the υ_{6a} mode is possibly a good indicator of the strength of the N−M bond in the vibrational spectra.

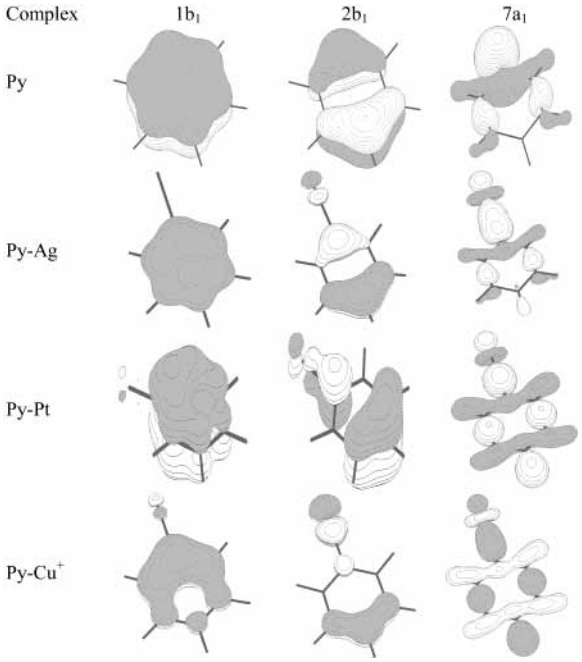

Figure 7. Comparison in the bonding orbital electron cloud densities between the free pyridine, Py−Ag, Py−Pt, and Py−Cu^+ complexes.

The frequency dependence on the force constant of S_8 shown in Figure 5i again demonstrates that the coupling among the υ_1, υ_{12}, and υ_{18a} modes is lost in Py−Cu^+. Since the results in the Py−M^+ complexes are similar to each other. Results on Py−Ag^+ and Py−Au^+ are not discussed here.

Orbital Shapes and Electronic Structures. Contour maps of the π bonding ($1b_1$, $2b_1$) and the lone pair ($7a_1$) orbitals of Py−M^{δ} are given in Figure 7. The contour maps of the corresponding orbitals of the free pyridine are also given in Figure 7 for comparison. The orbitals of $7a_1$ are mainly contributed by the lone pair orbital on the nitrogen of pyridine. After bonding between pyridine and a metal atom or ion, there is clearly an overlap of the lone pair of electrons on nitrogen and the s−d_σ hybride orbital of the metal. The orbitals of $1b_1$ and $2b_1$ are bonding orbitals involved in the first and second π-bonds of pyridine. Because of the different bonding nature, the shape of the $2b_1$ orbital has an increased deformation from Py−Ag through Py−Pt to Py−Cu^+. The electron density of the $2b_1$ orbital disappears at the $C_2-N_1-C_6$ moiety due to the strong electrostatic polarization. Simultaneously, the polarization effect also results in an electron deficiency of the $1b_1$ orbital at the C_4 position of the pyridine ring. This suggests that to a certain degree the electrostatic effect breaks out of the conjugation effect of the pyridine ring.[13,15]

Concluding Remarks

Density functional theory at the level of B3YLP/6-311+G** (for C, N, H)/LANL2DZ (for M) has been used for the normal-mode analysis of the neutral and cationic ion species of pyridine−metal atom (ion) complexes. The binding energies between pyridine and the metal atoms or ions have been analyzed in terms of the σ-donation and the π-back-donation. The Py−Ag complex is characterized by the weak σ-donation/π-back-donation interactions. The structural parameters of the pyridine moiety in Py−Ag change slightly, resulting in a small frequency shift, which is found in the experimental Raman or infrared spectra of pyridine adsorbed on the silver surface. Contrarily, the σ-donation/π-back-donation interactions are strong in the transition-metal Pt−pyridine complex. The C−N bond distance significantly lengthens and the two C−C bonds parallel to each other shorten. The frequency shift is large due to the strong N−Pt bonding. The bonding between pyridine and Cu (or Au) is within the limits of the Py−Ag and the Py−Pt complexes. In the ion complexes Py−M^+, the electrostatic interaction makes a large contribution to the Py−M^+ binding energies. The bonding properties are considerably different from the neutral Py−M complexes. The π orbitals of pyridine are polarized due to the strong electrostatic polarization. The vibrational frequency shift is very sensitive to the type of the bonding between pyridine and metals (ions).

Based on the present calculations, new assignments of the fundamental frequencies for the bands attributed to the υ_{17a}, υ_3, υ_5, and υ_{18b} modes of the free pyridine in the reported infrared and Raman spectra have been suggested. The calculated frequency shifts have indicated that the coupling of υ_1, υ_{12}, and υ_{18a} modes depends on the strength of the N-metal bond and its bonding properties. The strong electrostatic effect decouples the υ_1, υ_{12}, and υ_{18a} modes. The frequency of the ring breathing mode υ_1 is sensitive to the structural changes from the weak σ-donation through the large σ-donation/π-back-donation to the interactions including the donation/back-donation and the electrostatic effect. The PEDs of the υ_{12} mode (1035 cm^{-1}) vary substantially as pyridine is interacting with different metals. It indicates that PEDs of υ_{12} should be quite different for pyridine in the liquid, in the complexes, or for pyridine adsorbed on the surfaces. This is in good agreement with the normal and the surface-enhanced Raman spectra of pyridine. The fundamental frequency of the υ_{6a} mode has a nearly linear relationship with the change of the force constant of the N−M bond. Accordingly, the frequency shift of υ_{6a} can be used to correlate directly to the strength of the interaction of pyridine with the metal atom (surface).

It has been shown that the SERS spectral feature is rather complex and cannot be interpreted simply by the SERS mechanism. One has to investigate the surface bonding behavior and recheck the assignment of vibrational properties of pyridine. The quantum chemical calculation would be helpful to assign properly the vibrational modes and to explain surface vibrational spectra of pyridine adsorbed at surfaces.

Acknowledgment. This work was supported by the Natural Science Foundation of China (20003008, 20023001, 20021002) and Fok Ying-Tung Educational Foundation.

References and Notes

(1) Harris, D. C.; Bertolucci, M. D. *Symmetry and Spectroscopy: An Introduction to Vibrational and Electronic Spectroscopy*; Dover Publication, Inc.: New York, 1989.

(2) Ibach, H.; Mills, D. L. *Electron Energy Loss Spectroscopy and Surface Vibrations*; Academic Press: New York, 1982.

(3) Shen, Y. R. *Nature* **1989**, *337*, 519. (b) Shen, Y. R. *The Principles of Nonlinear Optics*; Wiley: New York, 1984. (c) Melendres, C. A.; Tadjeddine, A. *Synchrotron Techniques in Interfacial Electrochemistry*; NATO Advanced Study Institute Series C432: Mathematical and Physical Sciences; Plenum: New York, 1994. (d) Bain, C. D. *J. Chem. Soc.-Faraday Trans.* **1995**, *91*, 1281.

(4) Gahl, C.; Ishioka, K.; Zhong, Q.; Hotzel, A.; Wolf, M. *Faraday Discussion* **2001**, *117*, 191.

(5) (a)Cohen, M. R.; Merrill, R. P. *Surf. Sci.* **1991**, *245*, 1. (b) Katayama, K.; Shibamoto, K.; Sawada, T. *Chem. Phys. Lett.* **2001**, *345*, 265. (c) Fedurco, M.; Augustynski, J. *Colloid. Surf. A* **1998**, *134*, 95. (d) Fedurco, M.; Augustynski, J. *Colloid. Surf. A* **1998**, *134*, 95. (e) Lauhon, L. J.; Ho, W. *J. Phys. Chem. A* **2000**, *104*, 2463. (f) Lee, J.-G.; Ahner, J.; Yates, J. T., Jr. *J. Chem. Phys.* **2001**, *114*, 1414. (g) Haq, S.; King, D. A. *J. Phys. Chem.* **1996**, *100*, 16957. (h) Komiyama, M.; Kobayashi, M. *J. Phys. Chem. B* **1999**, *103*, 10651. (i) Andersson, M. P.; Uvdal, P. *J. Phys. Chem. B* **2001**, *105*, 9458.

(6) (a) Otto, A.; Frank, K. H.; Reihl, B. *Surf. Sci.* **1985**, *163*, 140. (b) Zylka, G.; Otto, A. *Surf. Sci.* **2001**, *475*, 118.

(7) (a) Creighton, J. A.; Nltachford, Ch. G.; Albrecht, M. G. *J. Chem. Soc., Faraday Trans. 2* **1979**, *75*, 790. (b) Creighton, J. A. *Surf. Sci.* **1985**, *158*, 211.

(8) (a) Arenas, J. F.; Lopez-Tocon, I.; Otero, J. C.; Marcos, J. I. *J. Phys. Chem.* **1996**, *100*, 9254. (b) Lopez-Tocon, I.; Centeno, S. P.; Otero, J. C.; Marcos, J. I. *J. Mol. Struct.* **2001**, *565/566*, 369.

(9) Rubim, J. C.; Corio, P.; Ribeiro, M. C. C.; Matz, M. *J. Phys. Chem.* **1995**, *99*, 15765.

(10) Stern, D. A.; Laguren-Davidson, L.; Frank, D. G.; Gui, J. Y.; Lin, C.; Lu, F.; Salaita, G. N.; Walton, N.; Zapien, D. C.; Hubbard, A. T. *J. Am. Chem. Soc.* **1989**, *111*, 877.

(11) Yamada, H.; Yamamoto, Y. *Surf. Sci.* **1983**, *134*, 71.

(12) Aramaki, K.; Ohi, M.; Uehara, J. *J. Electrochem. Soc.* **1992**, *139*, 1525.

(13) Ajito, K.; Takahashi, M.; Ito, M. *Chem. Phys. Lett.* **1989**, *158*, 193.

(14) Mizutani, G.; Ushioda, S. *J. Chem. Phys.* **1989**, *91*, 598.

(15) Ferwerda, R.; van der Maas, J. H.; van Duijneveldt, F. B. *J. Mol. Catal. A* **1996**, *104*, 319.

(16) (a) Nie, S.; Emory, S. R. *Science* **1997**, *275*, 1102. (b) Emory, S. R.; Nie, S. *J. Am. Chem. Soc.* **1998**, *120*, 8009. (c) Krug, J. T.; Wang, G. D.; Emory, S. R.; Nie, S. *J. Am. Chem. Soc.* **1999**, *121*, 9208.

(17) (a) Kneipp, K.; Wang, Y.; Kneipp, H.; Perelman, L. T.; Itzkan, I.; Dasari, R. R.; Feld, M. S. *Phys. Rev. Lett.* **1997**, *78*, 1667−1670. (b) Kneipp, K.; Kneipp, H.; Itzkan, I.; Dasari, R. R.; Feld, M. S. *Chem. Rev.* **1999**, *99*, 2957. (c) Kneipp, K.; Harrison, G. R.; Emory, S. R.; Nie, S. *Chimia* **1999**, *53*, 35.

(18) Destexhe, A.; Smets, J.; Adamowicz, L.; Maes, G. *J. Phys. Chem.* **1994**, *98*, 1506.

(19) Dkhissi, A.; Adamowicz, L.; Maes, G. *J. Phys. Chem. A* **2000**, *104*, 2112.

(20) Papai, I.; Jancso, G. *J. Phys. Chem. A* **2000**, *104*, 2132.

(21) Schlucker, S.; Sighn, R. K.; Asthana, B. P.; Popp, J.; Kiefer, W. *J. Phys. Chem. A* **2001**, *105*, 9983.

(22) Takahashi, H.; Mamola, K.; Plyler, E. K. *J. Mol. Spectrosc.* **1966**, *21*, 217.

(23) Asthana, B. P.; Takahashi, H.; Kiefer, W. *Chem. Phys. Lett.* **1983**, *94*, 41.

(24) Kreyenschmidt, M.; Eysel, H. H.; Asthana, B. P. *J. Raman Spectrosc.* **1993**, *24*, 645.

(25) Cabaco, M. I.; Besnard, M.; Yarwood, J. *Mol. Phys.* **1992**, *50*, 139.

(26) Zoidis, E.; Yarwood, J.; Danten, Y.; Besnard, M. *Mol. Phys.* **1995**, *85*, 373.

(27) Deckert, V.; Asthana, B. P.; Mishra, P. C.; Kiefer, W. *J. Raman Spectrosc.* **1996**, *27*, 907.

(28) (a) Fleischmann, M.; Hendra, P. J.; McQuillan, A. J. *Chem. Phys. Lett.* **1974**, *26*, 163. (b) Jeanmaire, D. J.; Van Duyne, R. P. *J. Electroanal. Chem.* **1977**, *84*, 1. (c) Albrecht, M. G.; Creighton, J. A. *J. Am. Chem. Soc.* **1977**, *99*, 5215. (d) Billmann, J.; Otto, A. *Solid State Commun.* **1982**, *44*, 105. (e) Ueba, H.; Ichimura, S.; Yamada, H. *Surf. Sci.* **1982**, *119*, 433. (f) Parker, L. M.; Bibby, D. M.; Burns, G. R. *J. Chem. Soc., Faraday Trans.* **1991**, *87*, 3319. (g) Creighton, J. A. In *Progress in Surface Raman Spectroscopy-Theory, Technique and Applications*; Tian, Z. Q., Ren, B., Eds.; Xiamen University Press: Xiamen, 2000; pp 11−16.

(29) (a) Parry, E. P. *J. Catal.* **1963**, *2*, 371. (b) Van Duyne, R. P. In *Chemical and Biochemical Applications of Lasers*; Moore, C. B., Ed.; Academic Press: New York, 1979; Vol. 4, pp 101−185. (c) Fleischmann, M.; Hill, I. R. In *Comprehensive Treatise of Electrochemistry*; White, R. E., Bockris, J. O. M., Conway, B. E., Yeager, E., Eds.; Plenum Press: New York, 1984; Vol. 8, pp 373−432. (d) Birke, R. L.; Lu, T.; Lombardi, J. R. In *Techniques for Characterization of Electrodes and Electrochemical Processes*; Varma, R., Selman, J. R., Eds.; John Wiley & Sons: 1991; pp 211−277. (e) Wachs, I. E. *Catal. Today* **1996**, *27*, 437.

(30) Udagawa, M.; Chou, C.-C.; Hemminger, J. C.; Ushioda, S. *Phys. Rev. B* **1981**, *23*, 6843.

(31) Compion, A.; Mullins, D. R. *Surf. Sci.* **1985**, *158*, 263.

(32) Van Duyne, R. P. *J. Phys. (Paris)* **1977**, *38*, C5−239.

(33) Yamada, H. *Surf. Sci.* **1987**, *182*, 269.

(34) Temperini, M. L. A.; Chagas, H. C.; Sala, O. *Chem. Phys. Lett.* **1981**, *79*, 75.

(35) Bilmes, S. A.; Rubim, J. C.; Otto, A.; Arvia, A. J. *Chem. Phys. Lett.* **1989**, *159*, 89.

(36) Feilchenfeld, H.; Gao, X.; Weaver, M. J. *Chem. Phys. Lett.* **1989**, *161*, 321.

(37) (a) Ren, B.; Huang, Q. J.; Cai, W. B.; Mao, B. W.; Liu, F. M.; Tian, Z. Q. *J. Electroanal. Chem.* **1996**, *415*, 175. (b) Gao, J. S.; Tian, Z. Q. *Spectrochim. Acta A* **1997**, *53*, 1595. (c) Cao, P. G.; Yao, J. L.; Ren, B.; Mao, B. W.; Gu, R. A.; Tian, Z. Q. *Chem. Phys. Lett.* **2000**, *316*, 1. (d) Wu, D. Y.; Xie, Y.; Ren, B.; Yan, J. W.; Mao, B. W.; Tian, Z. Q. *Phys. Chem. Commun.* **2001**, *18*, 1.

(38) Cai, W. B.; Ren, B.; Li, X. Q.; She, C. X.; Liu, F. M.; Cai, X. W.; Tian, Z. Q. *Surf. Sci.* **1998**, *406*, 9.

(39) (a) Gu, R. A.; Cao, P. G.; Yao, J. L.; Ren, B.; Xie, Y.; Mao, B. W.; Tian, Z. Q. *J. Electroanal. Chem.* **2001**, *505*, 95. (b) Cao, P. G.; Sun, Y. H.; Yao, J. L.; Ren, B.; Gu, R. A.; Tian, Z. Q. *Langmuir* **2002**, *18*, 2737.

(40) Tian, Z. Q.; Ren, B. In *Encyclopedia of Analytical Chemistry*; Meyers, R. A., Ed.; Wiley & Sons: Chichester, U.K., 2000; p 9162.

(41) Tian, Z. Q.; Ren, B.; Wu, D. Y. *J. Phys. Chem. B*, in press.

(42) Frisch, M. J.; Trucks, G. W.; Schlegel, H. B.; Gill, P. M. W.; Johnson, B. G.; Robb, M. A.; Cheeseman, J. R.; Keith, T. A.; Petersson, G. A.; Montgomery, J. A.; Raghavachari, K.; Al-Laham, M. A.; Zakrzewski, V. G.; Ortiz, J. V.; Foresman, J. B.; Cioslowski, J.; Stefanov, B. B.; Nanayakkara, A.; Challacombe, M.; Peng, C. Y.; Ayala, P. Y.; Chen, W.; Wong, M. W.; Andres, J. L.; Replogle, E. S.; Gomperts, R.; Martin, R. L.; Fox, D. J.; Binkley, J. S.; Defrees, D. J.; Baker, J.; Stewart, J. P.; Head-Gordon, M.; Gonzales, C.; Pople, J. A. *Gaussian 98*; Gaussian Inc.: Pittsburgh, PA, 1998.

(43) Becke, A. D. *J. Chem. Phys.* **1993**, *98*, 5648.

(44) (a) Hay, P. J.; Wadt, W. R. *J. Chem. Phys.* **1985**, *82*, 270. (b) Wadt, W. R.; Hay, P. J. *J. Chem. Phys.* **1985**, *82*, 284. (c) Hay, P. J.; Wadt, W. R. *J. Chem. Phys.* **1985**, *82*, 299.

(45) Moore, C. E. *Atomic Energy Levels as Derived from the Analysis of Optical Spectra*; U.S. Government Printing Office: Washington, DC, 1971; Vol. III, pp 38−43, 181−185.

(46) Smith, G. W.; Carter, E. A. *J. Phys. Chem.* **1991**, *95*, 2327.

(47) Reed, A. E.; Curtiss, L. A.; Weinhold, F. *Chem. Rev.* **1988**, *88*, 899.

(48) Pulay, P.; Fogarasi, G.; Pang, F.; Boggs, J. E. *J. Am. Chem. Soc.* **1979**, *101*, 2550.

(49) Wiberg, K. B.; Walters, V. A.; Wong, K. N.; Colson, S. D. *J. Phys. Chem.* **1984**, *88*, 6067.

(50) Pongor, G.; Pulay, P.; Fogarasi, G.; Boggs, J. E. *J. Am. Chem. Soc.* **1984**, *106*, 2765.

(51) Pongor, G.; Fogarasi, G.; Boggs, J. E.; Pulay, P. *J. Mol. Spectrosc.* **1985**, *114*, 445.

(52) Xue, Y.; Xie, D.; Yan, G. *Int. J. Quantum Chem.* **2000**, *76*, 686.

(53) Klots, T. D. *Spectrochim. Acta A* **1998**, *54*, 1481 and references therein.

(54) Wilson, E. B.; Decius, J. C.; Cross, P. C. *Molecular Vibration*; McGraw-Hill: New York, 1955.

(55) Herzberg, G. In *Molecular Spectra and Molecular Structure: II. Infrared and Raman Spectra of Polyatomic Molecules*; Van Nostrand Weinhold Co.: New York, 1945; p 214.

(56) Sharma, S. D.; Doraiswamy, S. *Chem. Phys. Lett.* **1976**, *41*, 192.

(57) Innes, K. K.; Ross, I. G.; Moomaw, W. R. *J. Mol. Spectrosc.* **1988**, *132*, 492.

(58) Martin, J. M. L.; Alsenoy, C. V. *J. Phys. Chem.* **1996**, *100*, 6973.

(59) Lupinetti, A. J.; Fau, S.; Frenking, G.; Strauss, S. H. *J. Phys. Chem. A* **1997**, *101*, 9551.

(60) Tadjeddine, M.; Flament, J. P. *Chem. Phys.* **2001**, *265*, 27.

(61) Arenas, J. F.; Tocon, I. L.; Otero, J. C.; Marcos, J. I. *J. Mol. Struct.* **1999**, *476*, 139.

(62) Walters, V. A.; Snavely, D. L.; Colson, S. D.; Wiberg, K. B.; Wong, K. N. *J. Phys. Chem.* **1986**, *90*, 592.

(63) Castellucci, E.; Sbrana, G.; Verderame, E. D. *J. Chem. Phys.* **1969**, *51*, 3762.

(64) DiLella, D. P.; Stidham, H. D. *J. Raman Spectrosc.* **1980**, *9*, 90.

(65) Stidham, H. D.; DiLella, D. P. *J. Raman Spectrosc.* **1980**, *9*, 247.

(66) Yang, W.-H.; Schatz, G. C. *J. Chem. Phys.* **1992**, *97*, 3831.

(67) Wong, K.; Colson, S. D. *J. Mol. Spectrosc.* **1984**, *104*, 129.

(68) Wetzel, H.; Gerischer, H.; Pettinger, B. *Chem. Phys. Lett.* **1981**, *78*, 392.

(69) Yang, M. C.; Rockey, T. J.; Pursell, D.; Dai, H. L. *J. Phys. Chem. B* **2001**, *105*, 11945.

(70) Creighton, J. A.; Alvarez, M. S.; Weltz, D. A.; Garoff, S.; Kim, M. W. *J. Phys. Chem.* **1983**, *87*, 4793.

(71) Grassian, V. H.; Muetterties, E. L. *J. Phys. Chem.* **1986**, *90*, 5900.